A STRATEGY TO ELIMINATE INSTANTANEOUS ACTIVE POWER OSCILLATIONS AND REDUCE HIGH CURRENTS IN THE DFIG DURING ASYMMETRIC VOLTAGE SAGS

Joacillo L. Dantas[1], Paulo H. P. Silva[2], Jean M. L. Fonseca[2], Carlos G. C. Branco[2], Francisco K. de A. Lima[2]

[1]Federal Institute of Education, Science and Technology of Ceara, Fortaleza – Ceara, Brazil

[2]Department of Electrical Engineering, Federal University of Ceara, Fortaleza – Ceara, Brazil

e-mail: joacillo@ifce.edu.br, klima@dee.ufc.br, paulo.henrique1402@gmail.com, jlobodaf@alu.ufc.br, gustavo@dee.ufc.br

***Abstract* – Wind turbines are widespread around the globe, and the number of wind farms connected to the grid is continually increasing. The Doubly-Fed Induction Generator (DFIG) plays an important role, since it is one of the most used configurations for wind power generation. DFIG-based wind plants, however, are very sensitive to grid disturbances, specially to voltage sags, as these machines have their stator circuit directly connected to the grid. Voltage sags can result in oscillations in active power, torque and DC link voltage, as well as damage the machine and the back-to-back converter due to high currents that arise in such type of contingency. This work proposes a control strategy applied to the rotor-side converter (RSC) of the DFIG, in order to protect the machine and the back-to-back converter during voltage sags. The aim of the control strategy is to reduce the machine currents and also to remove the oscillating active power caused by unbalanced voltage sags.**

***Keywords* – Doubly-fed induction generator, Instantaneous active and reactive power, Unbalanced voltage sag, Wind power generation.**

NOMENCLATURE

Variables	
i, I	Instantaneous and rms current.
v, V	Instantaneous and rms voltage.
L	Inductance.
p	Instantaneous active power.
q	Instantaneous reactive power.
R	Resistence.
ω	Angular frequency.
θ	Angle.
ψ	Flux.
Subscripts	
$X_{d,q}$	Direct and quadrature reference axis.
X_r	Rotor.
X_s	Stator.
X_m	Magnetization.
X_{sag}	Sag.
X_0	Zero sequence.
Superscripts	
$X^{+,-}$	Positive and negative sequence.
X^*	Reference value.
$\bar{X}$	Average value.
$\tilde{X}$	Oscillating value.
$\vec{X}$	Vector.

Manuscript received 18/07/2018; first revision 28/11/2018; accepted for publication 26/02/2019, by recommendation of Editor Marcello Mezaroba. http://dx.doi.org/10.18618/REP.2019.2.0021

I. INTRODUCTION

Doubly fed induction generator (DFIG) based wind turbines are widespread in wind farms around the world. Its reduced size converter requirement makes them more cost effective compared to other variable speed systems [1], [2], however, it has the disadvantage of being extremely sensitive to grid voltage disturbances as the stator circuit is directly connected to the grid [3]–[5]. From these disturbances, voltage sags are specially harmful to DFIGs, and, it is important to highlight that the majority of them are unbalanced, with single-phase voltage sags alone being responsible for 75% of all sag occurrences [6]–[8]. Asymmetric voltage sags cause unbalanced currents, resulting in torque pulsations and oscillations in the DFIG active and reactive power [9]–[14]. These scenarios increase the mechanical stress and DC link voltage oscillations. Whenever a voltage sag occurs, the stator magnetic flux might comprise positive, negative and zero sequence components which can cause rotor overvoltages, and rotor and stator overcurrents [2], [4], [15], [16]. Therefore, it is necessary to develop a control strategy to protect the machine and the converters from the destructive currents that emerge in the occurrence of voltage sags.

In the literature it is possible to find several strategies used to solve this problem. [17]–[32].

One well-known strategy is the use of a crowbar circuit, where resistors are connected to the rotor windings in order to damp the rotor magnetic flux [17]–[19], [27]. Although such circuit limits short-circuit currents, it does not allow the rotor-side converter (RSC) to control machine active and reactive power. This limitation encouraged researchers to seek crowbarless configurations, such as the ones controlling the RSC [20]–[26], [28]–[30], [32].

Dantas in [8] and Karimi in [31] present techniques for fast fault detection. These methods are useful for the proposed compensation system to act accurately, however, alone, they are not tools to bypass the problems caused by the voltage sag.

This paper explores a control strategy applied to the RSC by controlling the reactive and active power thorugh the Field Oriented Control (FOC) technique. The goal is to suppress

oscillations in the active power and reduce the high currents emerging from voltage sags, thus protecting the DFIG.

This work is presented as follows: Section II shows the classical DFIG modeling with control applied to the RSC and reactive and active power as control references. In Section III, the equations for the DFIG operation under voltage sag are derived and, in Section IV, the calculations of the current references to cancel out the oscillations of the active power are displayed. Section V presents the proposed control strategy and, lastly, Section VI presents experimental results.

II. DFIG: CLASSIC VECTOR CONTROL STRATEGY APPLIED TO THE ROTOR-SIDE CONVERTER

The stator active and reactive power can be controlled by the RSC using *field-oriented control* (FOC) in the dq reference frame (positive components rotate clockwise, negative rotate counterclockwise). In this strategy, the d-axis is aligned with the stator flux vector, as shown in [5]. Neglecting the stator winding resistance, and considering the stator voltage vector leading the magnetic flux by 90°, result $\psi_{sd} = |\vec{\psi}_s|$ and $\psi_{sq} = 0$. Thus:

$$i_{sd} = \frac{\psi_{sd}}{L_s} - \frac{L_m}{L_s} i_{rd}, \tag{1}$$

and

$$i_{sq} = -\frac{L_m}{L_s} i_{rq}. \tag{2}$$

Knowing that $\psi_s = v_{sq}/\omega_s$, the stator active and reactive power, according to [33], are given by:

$$p_s = \frac{3}{2}(v_{sd} i_{sd} + v_{sq} i_{sq}) \tag{3}$$

and

$$q_s = \frac{3}{2}(v_{sq} i_{sd} - v_{sd} i_{sq}), \tag{4}$$

becoming

$$p_s = -\frac{3}{2}\frac{L_m}{L_s} v_{sq} i_{rq}, \tag{5}$$

and

$$q_s = \frac{3}{2}\frac{L_m}{L_s}\left(\frac{v_{sq}^2}{\omega_s L_m} - v_{sq} i_{rd}\right). \tag{6}$$

III. DFIG UNDER UNBALANCED VOLTAGE

In three-phase systems the instantaneous active and reactive power can be decomposed in average and oscillating components, as stated by p-q theory [33]. Ignoring the harmonics dependent components, they can be written as:

$$\begin{aligned}
\bar{p} &= 3V^+I^+cos(\theta_{v+} - \theta_{i+}) + 3V^-I^-cos(\theta_{v-} - \theta_{i-}),\\
\bar{q} &= 3V^+I^+sen(\theta_{v+} - \theta_{i+}) - 3V^-I^-sen(\theta_{v-} - \theta_{i-}),\\
\tilde{p} &= -3V^+I^-cos(2\omega t + \theta_{v+} + \theta_{i-})\\
&\quad -3V^-I^+cos(2\omega t + \theta_{v-} + \theta_{i+}),\\
\tilde{q} &= -3V^+I^-sen(2\omega t + \theta_{v+} + \theta_{i-})\\
&\quad +3V^-I^+sen(2\omega t + \theta_{v-} + \theta_{i+}),\\
p_0 &= 3V_0I_0cos(\theta_{v0} - \theta_{i0}) - 3V_0I_0cos(2\omega t + \theta_{v0} + \theta_{i0}).
\end{aligned} \tag{7}$$

Taking into consideration a three-phase unbalanced system with only three conductors, as in the case of the DFIG under unbalanced voltage sag, the zero-sequence current component is not present, thus the instantaneous zero-phase sequence power is equal to zero ($p_0 = 0$). The average instantaneous active and reactive powers ($\bar{p}$, $\bar{q}$) come from the interaction between voltages and currents of same sequence, whereas oscillating components ($\tilde{p}, \tilde{q}$) are originated from interaction between voltages and currents of different sequences.

$$p_s + jq_s = \frac{3}{2}(v_{sdq}^+ e^{j\omega t} + v_{sdq}^- e^{-j\omega t})(i_{sdq}^+ e^{j\omega t} + i_{sdq}^- e^{-j\omega t})^*. \tag{8}$$

The instantaneous active and reactive power can be obtained by manipulating (8). Furthermore, the oscillating components are represented by two parts, the first one as a function of a cosine (P_{c2} and Q_{c2}) and the second one as a function of a sine (P_{s2} and Q_{s2}), both oscillating at twice the grid frequency:

$$p = \bar{p} + P_{c2}cos(2\omega t) + P_{s2}sen(2\omega t), \tag{9}$$

and

$$q = \bar{q} + Q_{c2}cos(2\omega t) + Q_{s2}sen(2\omega t). \tag{10}$$

The coefficients are given by:

$$\begin{aligned}
\bar{p} &= \frac{3}{2}(v_{sd}^+ i_{sd}^+ + v_{sq}^+ i_{sq}^+ + v_{sd}^- i_{sd}^- + v_{sq}^- i_{sq}^-),\\
P_{c2} &= \frac{3}{2}(v_{sd}^+ i_{sd}^- + v_{sq}^+ i_{sq}^- + v_{sd}^- i_{sd}^+ + v_{sq}^- i_{sq}^+),\\
P_{s2} &= \frac{3}{2}(v_{sq}^- i_{sd}^+ - v_{sd}^- i_{sq}^+ - v_{sq}^+ i_{sd}^- + v_{sd}^+ i_{sq}^-),\\
\bar{q} &= \frac{3}{2}(v_{sq}^+ i_{sd}^+ - v_{sd}^+ i_{sq}^+ + v_{sq}^- i_{sd}^- - v_{sd}^- i_{sq}^-),\\
Q_{c2} &= \frac{3}{2}(v_{sq}^+ i_{sd}^- - v_{sd}^+ i_{sq}^- + v_{sq}^- i_{sd}^+ - v_{sd}^- i_{sq}^+),\\
Q_{s2} &= \frac{3}{2}(v_{sd}^+ i_{sd}^- + v_{sq}^+ i_{sq}^- - v_{sd}^- i_{sd}^+ - v_{sq}^- i_{sq}^+).
\end{aligned} \tag{11}$$

The positive and negative sequences of the current and voltage are obtained from the Double Second-Order Generalized Integrator-Frequency Locked Loop (DSOGI-FLL) structure. This technique is well established in [34].

For both positive and negative synchronous reference frame, by aligning the d-axis with the stator flux vector, one has $v_{sd}^+ = 0$ and $v_{sd}^- = 0$. Isolating the average instantaneous active power, and, the component of the oscillating instantaneous active power that is function of a cosine, results in the following matrix expression:

$$\frac{2}{3}\begin{bmatrix} \bar{p} \\ P_{c2} \end{bmatrix} = \begin{bmatrix} v_{sq}^+ & v_{sq}^- \\ v_{sq}^- & v_{sq}^+ \end{bmatrix} \begin{bmatrix} i_{sq}^+ \\ i_{sq}^- \end{bmatrix}. \tag{12}$$

Similarly, isolating the average instantaneous reactive power and the component of the oscillating instantaneous active power which is function of a sine results in:

$$\frac{2}{3}\begin{bmatrix} \bar{q} \\ P_{s2} \end{bmatrix} = \begin{bmatrix} v_{sq}^+ & v_{sq}^- \\ v_{sq}^- & -v_{sq}^+ \end{bmatrix} \begin{bmatrix} i_{sd}^+ \\ i_{sd}^- \end{bmatrix}. \tag{13}$$

After algebraic manipulations the stator currents, in the positive and negative synchronous reference frame, can be expressed as:

$$\begin{aligned} i_{sq}^{+} &= \frac{2}{3\Delta}(\bar{p}.v_{sq}^{+} - P_{c2}.v_{sq}^{-}), \\ i_{sq}^{-} &= \frac{2}{3\Delta}(P_{c2}.v_{sq}^{+} - \bar{p}.v_{sq}^{-}), \end{aligned} \tag{14}$$

and

$$\begin{aligned} i_{sd}^{+} &= \frac{2}{3\delta}(\bar{q}.v_{sq}^{+} + P_{s2}.v_{sq}^{-}), \\ i_{sd}^{-} &= \frac{2}{3\delta}(\bar{q}.v_{sq}^{-} - P_{s2}.v_{sq}^{+}) \cdot \end{aligned} \tag{15}$$

Furthermore $\Delta = (v_{sq}^{+})^2 - (v_{sq}^{-})^2$ and $\delta = (v_{sq}^{+})^2 + (v_{sq}^{-})^2$.

It is important to highlight that for the scenario where the positive sequence of the stator voltage on the quadrature axis (v_{sq}^{+}) is equal to the negative sequence (v_{sq}^{-}), that is, when $\Delta = 0$, there will be a singularity. However, this case will occur only in a two-phase voltage interruption (e.g. $v_a = 1p.u.$ and $v_b = v_c = 0p.u.$), which is not addressed in this work, since it is on voltage sags. Furthermore, during voltage sags the positive sequence will most often have the largest modulus $(v_{sq}^{+})^2 > (v_{sq}^{+})^2$.

Lastly, if the power values presented in (14) and (15) are known, the stator currents can be determined.

IV. OBTAINING THE REFERENCE CURRENTS FOR THE DFIG OPERATION UNDER ASYMMETRIC VOLTAGE SAGS

An asymmetric voltage sag causes unbalanced voltages at the point of common coupling (PCC). Therefore, the equations described in section III. are valid for this conditions.

The control strategy proposed in this article seeks to eliminate the oscillations in the active power and to protect the DFIG using as reference the active and reactive powers, which are chosen so as to attenuate the effect of the high currents in the stator and rotor due to the voltage sag.

A. Reference Stator Currents

From (14) and (15) the following reference stator currents are found:

$$\begin{aligned} i_{sq}^{+*} &= \frac{2}{3\Delta}(\bar{p}_{sag}.v_{sq}^{+}), \\ i_{sq}^{-*} &= \frac{2}{3\Delta}(-\bar{p}_{sag}.v_{sq}^{-}), \end{aligned} \tag{16}$$

and

$$\begin{aligned} i_{sd}^{+*} &= \frac{2}{3\delta}(\bar{q}_{sag}.v_{sq}^{+}), \\ i_{sd}^{-*} &= \frac{2}{3\delta}(\bar{q}_{sag}.v_{sq}^{-}) \cdot \end{aligned} \tag{17}$$

Where $\bar{p}_{sag}$ and $\bar{q}_{sag}$ are the setpoints of the average instantaneous active and reactive power.

B. Reference Rotor Currents

From (1) and (2), one can find the following reference currents for the RSC:

$$\begin{aligned} i_{rd}^{+*} &= \frac{\psi_{sd}^{+} - L_s i_{sd}^{+*}}{Lm}, \\ i_{rd}^{-*} &= \frac{\psi_{sd}^{-} - L_s i_{sd}^{-*}}{Lm}, \\ i_{rq}^{+*} &= \frac{-L_s i_{sq}^{+*}}{Lm}, \\ i_{rq}^{-*} &= \frac{-L_s i_{sd}^{-*}}{Lm}. \end{aligned} \tag{18}$$

Where the positive and negative sequence components of the magnetic flux can be estimated by:

$$\begin{aligned} \psi_{sq}^{+} &= \frac{v_{sd}^{+}}{\omega_s}, \\ \psi_{sd}^{+} &= \frac{v_{sq}^{+}}{\omega_s}, \\ \psi_{sq}^{-} &= -\frac{v_{sd}^{-}}{\omega_s}, \\ \psi_{sd}^{-} &= -\frac{v_{sq}^{-}}{\omega_s}. \end{aligned} \tag{19}$$

The reference rotor currents, in the synchronous reference frame, are now determined through the reference current positive and negative components:

$$i_{rd}^{*} = i_{rd}^{+*} + i_{rd}^{-*} \tag{20}$$

$$i_{rq}^{*} = i_{rq}^{+*} + i_{rq}^{-*} \tag{21}$$

V. CONTROL STRATEGY

A. Rotor Current Loop Model

In the rotor current loop the dominant poles were canceled in order to determine the controller gains [35], both in the quadrature and direct axis. The RSC switching frequency is equal to $f_{ch} = 10$ kHz, and the converter transfer function can be modeled as a constant time delay T_{RSC}, which is determined by:

$$T_{RSC} = \frac{2}{f_{ch}}. \tag{22}$$

According to the adopted criterion, the controller gains are:

$$K_{ii} = \frac{R_r}{2T_{RSC}}, \tag{23}$$

and

$$K_{pi} = \frac{K_{ii}\sigma Lr}{R_r}. \tag{24}$$

Where $\sigma = 1 - \frac{L_m^2}{L_r L_s}$. Figure 1 shows the q-axis rotor current

loop control.

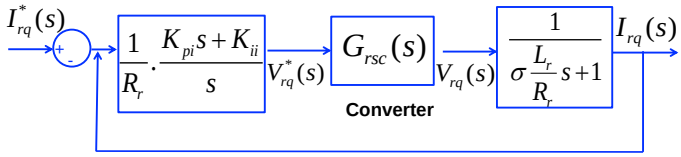

Fig. 1. Quadrature axis rotor current loop model.

B. Changing The Control Strategy From The Classic To The Proposed One

During balanced voltage the classic vector control was employed. The power control loops generate the reference currents to the current loops. After voltage sag detection, the control strategy shifts from the classic to the proposed control (see Figure 2). The algorithm presented in [8] was used to detect the voltage sags and to send the digital signal, named *vsd*, that was applied to change the control strategies in the high moments.

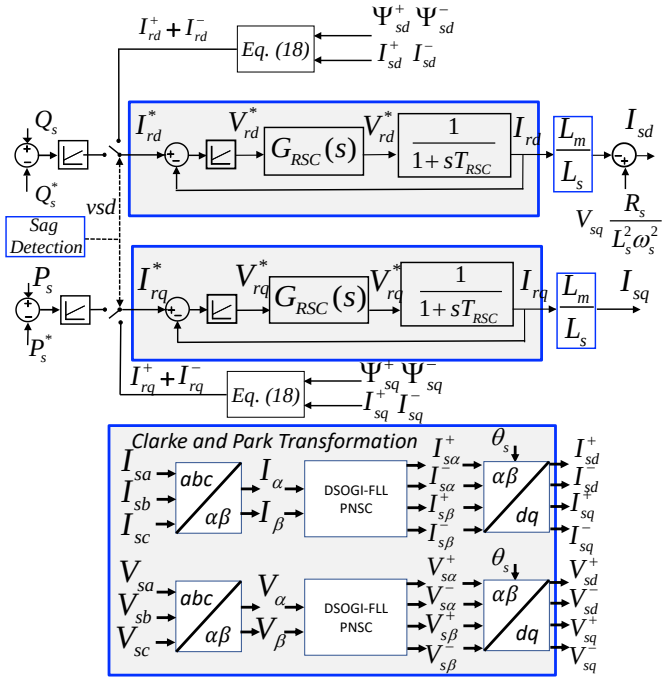

Fig. 2. Block diagram of the classic and proposed controls.

VI. EXPERIMENTAL RESULTS

In order to validate the proposed control strategy an experimental setup was assembled, where the DFIG was subject to voltage sags. A three-phase induction motor (TIM) driven by an inverter emulated the wind, and a three-phase rectifier was employed instead of the grid side converter (GSC). As consequence, the DFIG operated only in subsynchronous mode. Figure 3 details the system configuration, Table I and Table II show the DFIG and TIM parameters, respectively. Figure 4 exposes the experimental setup.

Following the requirements stated by *IEEE Std 1159-2009*, asymmetric voltage sags were manually imposed through a 10 kVA three-phase variable autotransformer connected between the grid and the DFIG. Two scenarios were considered for the validation; one-phase and two-phase voltage sag.

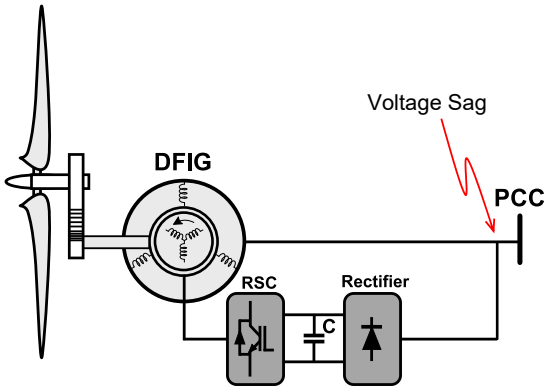

Fig. 3. Experimental setup representation.

TABLE I
DFIG Parameters

Parameters	Values
Rated Power	6kW/8kVA
Rated Voltage	380V
Frequency	60Hz
Stator Resistence	0.5417 Ω
Rotor Resistence	0.5815 Ω
Stator Leakage Inductance	5.00 mH
Rotor Leakage Inductance	6.5 mH
Magnetizing inductance	115.13 mH

TABLE II
TIM Parameters

Parameters	Values
Rated Power	10 hp
Rated Voltage	220/380/440V
Frequency	60Hz
Rated Current	25.1/ 14.9/12.9 A
Rotacional Speed	1750 rpm
Service Factor	1.15

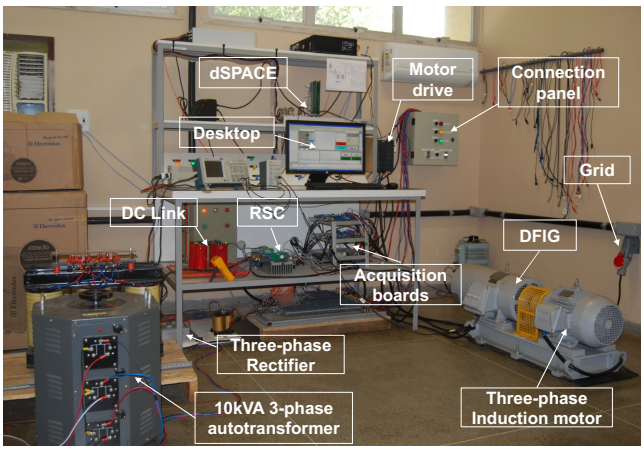

Fig. 4. Experimental setup.

A. Single-Phase Voltage Sag

Initially in steady state, the generator injects 2000 W active power and 0 var reactive power into the grid. Figure

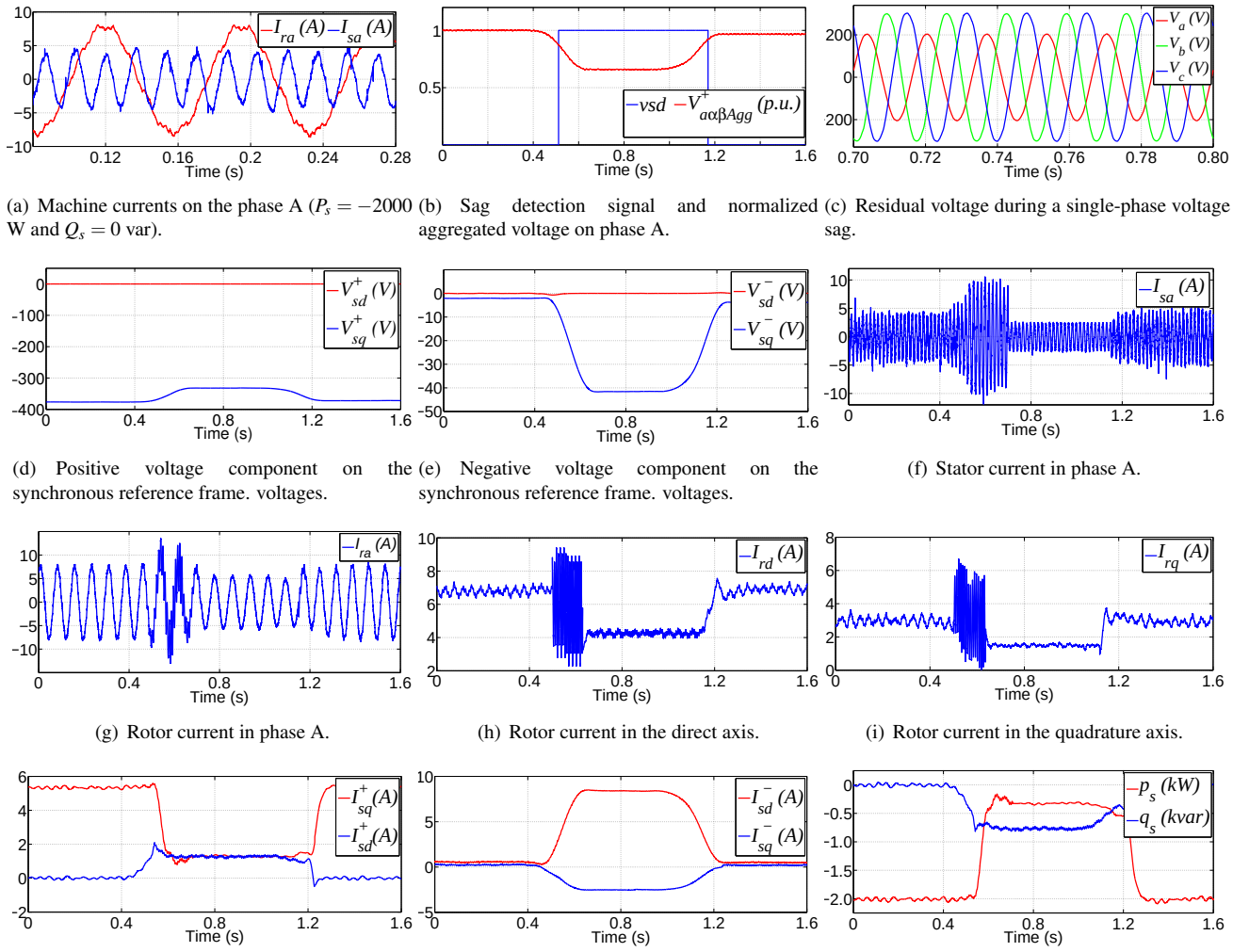

(a) Machine currents on the phase A ($P_s = -2000$ W and $Q_s = 0$ var).

(b) Sag detection signal and normalized aggregated voltage on phase A.

(c) Residual voltage during a single-phase voltage sag.

(d) Positive voltage component on the synchronous reference frame. voltages.

(e) Negative voltage component on the synchronous reference frame. voltages.

(f) Stator current in phase A.

(g) Rotor current in phase A.

(h) Rotor current in the direct axis.

(i) Rotor current in the quadrature axis.

(j) Positive sequence stator current in the synchronous reference frame.

(k) Negative sequence stator current in the synchronous reference frame .

(l) Instantaneous active and reactive power during the single-phase voltage sag.

Fig. 5. System response for single-phase voltage sag

5.a shows the DFIG currents in phase A at this operation point. The total harmonic distortion of the rotor and stator currents are 6.89% and 10.05%, respectively. The constructive characteristics of the machine bring about these distorted currents. Afterwards, a 0.66 $p.u.$ single-phase voltage sag was forced on phase A, as illustrated in Figure 5.b, which shows the digital signal detecting the sag as well as the normalized aggregate voltage on phase A, previously defined in [8] as $V^{+}_{a\alpha\beta Agg} = \sqrt{v^{+}_{a\alpha}(t)^2 + v^{+}_{a\beta}(t)^2}$.

The single-phase voltage sag generated positive, negative and zero sequence voltage components. Since the system considered has only three conductors, there is no interest in the zero sequence components. Figure 5.c depicts the residual voltages, and Figure 5.d and 5.e depict respectively the positive and negative voltage components on the synchronous reference frame. As the stator magnetic flux is aligned with the d-axis, $v^{+}_{sd} = 0$. Disregarding small oscillations on the negative sequence component in the beginning and in the end of the sag, $v^{-}_{sd} = 0$.

At the beginning of the voltage sag current oscillations are presented, as can be seen in Figure 5.f. This is more perceptible in the rotor current plot (Figure 5.g). As can be seen in both plots, the currents experience an increase and, after the proposed control strategy takes place, their amplitude become restricted and oscillations are eliminated.

When the DFIG injects 2000 W and 0 var into the grid, the rotor currents in the synchronous reference frame have average values of $I_{rd} = 6.8$ A and $I_{rq} = 3$ A (see Figures 5.h and 5.i). The reference values for the current loops are given by the

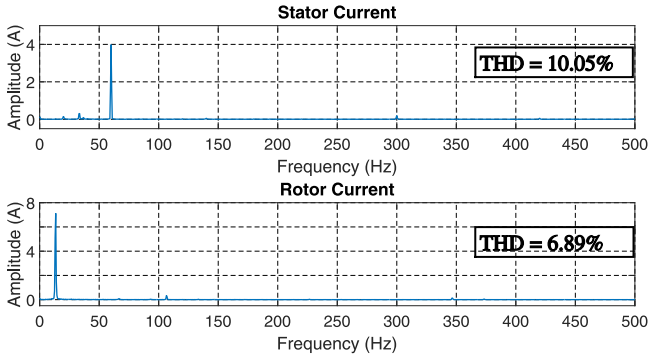

Fig. 6. Stator and rotor currents Fast-Fourier Transform.

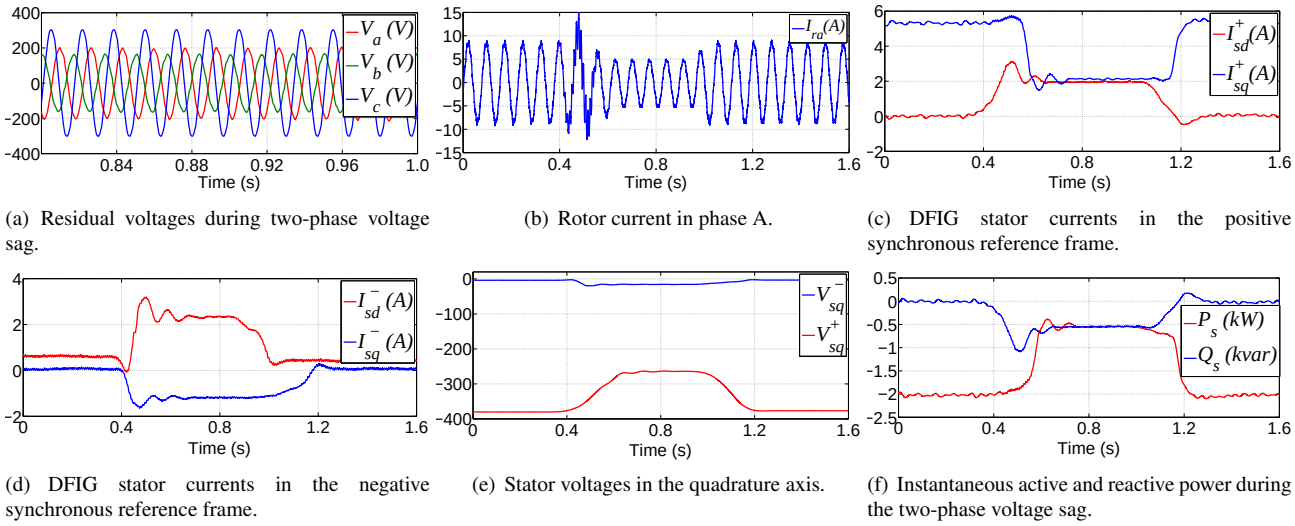

(a) Residual voltages during two-phase voltage sag.

(b) Rotor current in phase A.

(c) DFIG stator currents in the positive synchronous reference frame.

(d) DFIG stator currents in the negative synchronous reference frame.

(e) Stator voltages in the quadrature axis.

(f) Instantaneous active and reactive power during the two-phase voltage sag.

Fig. 7. System response for two-phase voltage sag.

power loop outputs. However, these references are given by the proposed control strategy when the voltage sag is detected. The power setpoints $p^* = \bar{p}_{sag} = -350$ W and $q^* = \bar{q}_{sag} = -750$ var were adopted for this experiment to reduce the high currents caused by voltage sag.

Although there is reactive power injection in the sag event, the rotor d-axis current decreases. The stator currents, shown in Figure 5.k, are a better evidence of the power injection.

From (11), one can write:

$$\bar{p} = v^+_{sq} i^+_{sq} + v^-_{sq} i^-_{sq}, \tag{25}$$

and also

$$\bar{q} = v^+_{sq} i^+_{sd} + v^-_{sq} i^-_{sd}. \tag{26}$$

Figure 5.l indicates the stator instantaneous active and reactive power, at which it is clearly seen that the oscillating components in the instantaneous active power caused by the unbalanced voltages are eliminated ($P_{s2} = P_{c2} = 0$).

As the grid side converter (GSC) is not present, the DC link voltage increases. This increase is due to the change in the active power reference from -2000 W to -350 W when the single-phase voltage sag happens. However, the proposed strategy does not allow DC link voltage oscillations. The variation of $\Delta P_s = 1650$ W in the inject active power forces the DC link capacitor to accumulate the exceeding energy. The DC link voltage augmented from 305 V to 315 V.

B. Two-Phase Voltage Sag

The variable autotransformer configurations were changed in order to impose voltage sag in phases A and B. Figure 7.a shows the residual voltages for this conditions. In this two-phase voltage sag experiment, the reference values for inject active and reactive power were $\bar{p}_{sag} = -500$ W and $\bar{q}_{sag} = -500$ var.

The rotor currents on phases A and B present high oscillations at the beginning of the sag, caused by the voltage unbalance, eventually disappearing after the action of the proposed control strategy. Figure 7.b exposes the current on phase A.

Analyzing the rotor currents in the synchronous reference frame, it can be observed that, for the positive sequence, the direct axis compensator of the current loop is slower and has more oscillations than the one in the quadrature axis. For the negative sequence, the compensator has even more oscillations, however the quadrature axis is slower, as shown in Figures 7.c and 7.d.

From (25) and (26), it is important to highlight the stator voltages in the quadrature axis waveforms (see Figure 7.e), since the stator average instantaneous active and reactive power are determined by them.

The experimental results obtained show that, despite initial oscillations, the instantaneous power, after the transient state, are very close to the references $\bar{p}_{sag}$ and $\bar{q}_{sag}$, as shown in Figure 7.f.

VII. CONCLUSIONS

Whenever subject to unbalanced voltage sags, the DFIG presents high currents and oscillations in active power and DC link voltage. This unexpected stress can damage the machine as well as the back-to-back converter. After reviewing the literature with respect to the DFIG under unbalanced grid conditions and asymmetric voltage sags, this paper proposed a control strategy, which is applied to the rotor-side converter, that aims to eliminate active power oscillating components and to reduce the machine currents, helping the DFIG to withstand adverse conditions and stay connected to the grid without damaging any component. The power setpoints, during voltage sags, are changed to the values stipulated by the proposed control strategy. The strategy was experimentally validated for single and two voltage sags.

It was observed that the DFIG rotor currents was distorted after the grid connection. This undesired behavior was attributed to the machine characteristics. The distortions were reflected to the grid stator currents, and therefore, were presented as oscillations in the active and reactive power. The proposed control strategy was shown to be efficient in eliminating oscillations in the active power caused by asymmetric voltage sags, as well as the reduction of the current

values in the stator and rotor, protecting the DFIG. Moreover, the power setpoint values assigned during voltage sags were successfully met. All voltage sags used in the experiments followed the IEEE Std 1159-2009.

ACKNOWLEDGEMENTS

The authors thank the Department of Electrical of Engineering of Federeal University of Ceara and the Laboratory of Applications of Power Electronics and Integration to Energy Systems (LAPIS) for the support to carry out the experiments.

REFERENCES

[1] S. Müller, M. Deicke, R. W. De Doncker, "Doubly Fed Induction Generator Systems for Wind Turbines", *IEEE Industry Application Magazine*, vol. 8, no. 3, pp. 26–33, June 2002, doi:10.1109/TPEL.2008.921157.

[2] G. Abad, J. Lopez, M. Rodriguez, L. Marroyo, G. Iwanski, *Doubly fed induction machine: modeling and control for wind energy generation*, vol. 85, John Wiley & Sons, 2011.

[3] E. A. Mohamed, Y. Qudaih, Y. Mitani, M. Ebeed, "Study the Different effects of SFCL and Outer Crowbar on Fault Ride-through Capability Enhancement of Wind Farms", *Energy Procedia*, vol. 100, pp. 127–136, November 2016.

[4] I. Boldea, *Variable Speed Generators*, Taylor e Francis, 2006.

[5] F. K. A. Lima, J. L. Dantas, C. G. C. Branco, "Reactive power control of DFIG-based wind turbine during voltage sag", *in IECON-38th Annual Conference on IEEE Industrial Electronics Society*, pp. 4321–4325, IEEE, October 2012.

[6] M. H. Bollen, M. H. Bollen, *Understanding power quality problems: voltage sags and interruptions*, vol. 445, IEEE press New York, 2000.

[7] J. A. Martinez, J. Martin-Arnedo, "Voltage Sag Studies in Distribution Networks - Part II: Voltage Sag Assessment", *IEEE Transactions on Power Delivery*, vol. 21, no. 3, pp. 1679–1688, June 2006.

[8] J. L. Dantas, F. K. A. Lima, C. G. C. Branco, J. M. Guerrero, J. C. Vasquez, "A robust and fast generic voltage sag detection technique", *in IEEE 13th Brazilian Power Electronics Conference and 1st Southern Power Electronics Conference (COBEP/SPEC)*, pp. 1–6, November 2015.

[9] P. Tourou, C. Sourkounis, "DFIG-based wind energy conversion systems under unbalanced voltage dips", *in Power Electronics, Electrical Drives, Automation and Motion (SPEEDAM), International Symposium on*, pp. 877–882, June 2014.

[10] J. Morren, J, S. W. H. De Haan, "Ridethrough of wind turbines with doubly-fed induction generator during a voltage dip", *Energy Conversion, IEEE Transactions on*, vol. 20, no. 2, pp. 435–441, May 2005, doi: 10.1109/TEC.2005.845526.

[11] D. Xie, Z. Xu, L. Yang, J. Ostergaard, Y. Xue, K. P. Wong, "A Comprehensive LVRT Control Strategy for DFIG Wind Turbines With Enhanced Reactive Power Support", *Power Systems, IEEE Transactions on*, vol. PP, no. 99, pp. 1–9, February 2013, doi: 10.1109/TPWRS.2013.2240707.

[12] J. Solís-Chaves, M. S. Barreto, M. B. Salles, V. M. Lira, R. V. Jacomini, A. J. Sguarezi Filho, "A direct power control for DFIG under a three phase symmetrical voltage sag condition", *Control Engineering Practice*, vol. 65, pp. 48–58, August 2017.

[13] N. Zhou, F. Sun, Q. Wang, X. Meng, "A flexible power control strategy for rotor-side converter of DFIG under unbalanced grid voltage sags", *International Journal of Electrical Power & Energy Systems*, vol. 90, pp. 64–75, September 2017.

[14] V. F. Mendes, H. Pereira, F. F. Matos, W. Hofmann, S. R. Silva, "Doubly-fed induction generator control during unbalanced grid conditions", *in IEEE 13th Brazilian Power Electronics Conference and 1st Southern Power Electronics Conference (COBEP/SPEC)*, pp. 1–6, February 2015.

[15] S. Xiao, G. Yang, H. Zhou, H. Geng, "An LVRT Control Strategy Based on Flux Linkage Tracking for DFIG-Based WECS", *Industrial Electronics, IEEE Transactions on*, vol. 60, no. 7, pp. 2820–2832, July 2013, doi:10.1109/TIE.2012.2205354.

[16] M. K. Döşoğlu, "A new approach for low voltage ride through capability in DFIG based wind farm", *International journal of electrical power & energy systems*, vol. 83, pp. 251–258, December 2016.

[17] J. J. Justo, F. Mwasilu, J.-W. Jung, "Enhanced crowbarless FRT strategy for DFIG based wind turbines under three-phase voltage dip", *Electric Power Systems Research*, vol. 142, pp. 215–226, January 2017.

[18] S. Yang, T. Zhou, D. Sun, Z. Xie, X. Zhang, "A SCR crowbar commutated with power converter for DFIG-based wind turbines", *International Journal of Electrical Power & Energy Systems*, vol. 81, pp. 87–103, October 2016.

[19] M. Gholizadeh, S. Tohidi, A. Oraee, H. Oraee, "Appropriate crowbar protection for improvement of brushless DFIG LVRT during asymmetrical voltage dips", *International Journal of Electrical Power & Energy Systems*, vol. 95, pp. 1–10, February 2018.

[20] F. K. A. Lima, A. Luna, P. Rodriguez, E. Watanabe, F. Blaabjerg, "Rotor Voltage Dynamics in the Doubly Fed Induction Generator During Grid Faults", *Power Electronics, IEEE Transactions on*, vol. 25, no. 1, pp. 118–130, August 2010, doi:10.1109/TPEL.2009.2025651.

[21] Y. Liao, H. Li, J. Yao, K. Zhuang, "Operation and control of a grid-connected DFIG-based wind turbine with series grid-side converter during network unbalance", *Electric Power Systems Research*, vol. 81, no. 1, pp. 228–236, January 2011.

[22] A. Luna, F. K. A. Lima, D. Santos, P. Rodriguez, E. H. Watanabe, S. Arnaltes, "Simplified Modeling of a DFIG for Transient Studies in Wind Power

Applications", *IEEE Transactions on Industrial Electronics*, vol. 58, no. 1, pp. 9–20, January 2011, doi: 10.1109/TIE.2010.2044131.

[23] A. E. Leon, J. M. Mauricio, J. A. Solsona, "Fault Ride-Through Enhancement of DFIG-Based Wind Generation Considering Unbalanced and Distorted Conditions", *Energy Conversion, IEEE Transactions on*, vol. 27, no. 3, pp. 775–783, June 2012, doi: 10.1109/TEC.2012.2204756.

[24] D. Ananth, G. N. Kumar, "Fault ride-through enhancement using an enhanced field oriented control technique for converters of grid connected DFIG and STATCOM for different types of faults", *ISA transactions*, vol. 62, pp. 2–18, May 2016.

[25] L. Xu, Y. Wang, "Dynamic modeling and control of DFIG-based wind turbines under unbalanced network conditions", *IEEE Transactions on Power Systems*, vol. 22, no. 1, pp. 314–323, February 2007.

[26] L. Xu, *et al.*, "Coordinated control of DFIG's rotor and grid side converters during network unbalance", *IEEE Transactions on Power Electronics PE*, vol. 23, no. 3, p. 1041, May 2008.

[27] J. P. da Costa, H. Pinheiro, "Controle do gerador de inducão duplamente alimentado durante distúrbios na rede elétrica: Crowbar ativo e suporte de reativos", *in Proc. XVII Brazilian Conf. Automatica*, pp. 01–07, 2008.

[28] A. Luna, F. Lima, P. Rodriguez, E. Watanabe, R. Teodorescu, "Comparison of power control strategies for DFIG wind turbines", *in Industrial Electronics, IECON. 34th Annual Conference of IEEE*, pp. 2131–2136, January 2008.

[29] D. Xiang, L. Ran, P. J. Tavner, S. Yang, "Control of a doubly fed induction generator in a wind turbine during grid fault ride-through", *IEEE Transactions on Energy Conversion*, vol. 21, no. 3, pp. 652–662, August 2006.

[30] F. d. A. Lima, E. Watanabe, P. Rodriguez, A. Luna, *et al.*, "Controle de gerador de inducão duplamente alimentado diante de afundamentos de tensão", *Eletrônica de Potência*, vol. 3, no. 14, pp. 189–199, August 2009.

[31] S. Karimi, A. Gaillard, P. Poure, S. Saadate, "FPGA-based real-time power converter failure diagnosis for wind energy conversion systems", *IEEE Transactions on Industrial Electronics*, vol. 55, no. 12, pp. 4299–4308, November 2008.

[32] J. P. da Costa, H. Pinheiro, "Nova estratÃ©gia de controle de alto desempenho para operaÃ§Ã£o do GIDA durante distÃºrbios assimÃ©tricos na rede elÃ©trica", *Revista EletrÃ´nica de PotÃªncia*, vol. 13, no. 4, pp. 305–315, November 2009.

[33] H. Akagi, E. H. Watanabe, M. Aredes, *Instantaneous Power Theory and Applications to Power Conditioning*, 2nd ed., John Wiley & Sons, Inc., New York, N.Y., 2007.

[34] R. Teodorescu, M. Liserre, P. Rodriguez, *Grid converters for photovoltaic and wind power systems*, vol. 29, John Wiley & Sons, 2011.

[35] G. F. Franklin, J. D. Powell, A. Emami-Naeini, Marroyo, *Feedback Control of Dynamic Systems*, Prentice-Hall, 2010.

BIOGRAPHIES

Joacillo Luz Dantas holds a Bachelor's Degree (1994), a Master's Degree (2006) and a PhD (2017) in Electrical Engineering from the Federal University of Ceara. He was a guest PhD student in the Department of Energy Technology (Aalborg University) from 2014 to 2015. He has been a professor at the Federal Institute of Education, Science and Technology of Ceara (IFCE) since 1993. His areas of interest are: Power Electronics, Renewable Energies, Electrical Machine Drives and Active Power Filters. Joacillo L. Dantas has been a member of SOBRAEP since 2015.

Francisco Kleber de A. Lima born on November 3, 1968 in Fortaleza, he is an Electrical Engineer (1998) and a Master's Degree in Electrical Engineering (2003), by the University Federal of CearÃ¡. He holds a PhD in Electrical Engineering from COPPE/Federal University of Rio de Janeiro in 2009. He is a professor in the Department of Electrical Engineering at the Federal University of CearÃ¡. His areas of interest are: Power Electronics, Power Quality, Electric Machine Drives and Active Filtration. Dr. Francisco Kleber de A. Lima has been a member of SOBRAEP since 2002.

Paulo Henrique P. Silva born in Brasilia on February 14, 1987, he holds a Bachelor's degree in Physics from the State University of Ceara (2011), a Master's degree in Nuclear Engineering from the Military Engineering Institute (2013) and is currently a PhD student in the Graduate Program in Electrical Engineering by Federal University of Ceara. He is interested in the area of Alternative Energies and its applications, especially in wind, solar and nuclear energy, studying mainly the following subjects: Doubly Fed Induction Generator (DFIG), Power Quality, FACTS devices, Fast Spectrum Nuclear Reactor, Energy Matrices and Energy Efficiency.

Jean M. Lobo da Fonseca holds a Bachelor's degree in Electrical Engineering from the Federal University of Ceara (2017). He is currently pursing his Master's degree at the same university. His research interests are Grid Synchronization, FACTS Devices and Wind Power Generation.

Carlos Gustavo C. Branco holds a Bachelor's Degree in Electrical Engineering from the Federal University of CearÃ¡ (2002) and a Master's Degree in Electrical Engineering from the same university (2005). Since 2005 he has been working in the Research and Development area of High Frequency Isolated UPS Systems, Photovoltaic Power Systems and Machine Drives. Dr. Branco is currently an assistant professor in the Department of Electrical Engineering at the Federal University of CearÃ¡ and a member of IEEE and SOBRAEP.